



A highly sensitive near-infrared ratiometric fluorescent probe for imaging of mitochondrial hydrazine in cells and in mice models

Yaqun Song^a, Guang Chen^{a,c,*}, Xiaoyue Han^{a,b}, Jinmao You^{a,*}, Fabiao Yu^{a,b,*}

^a The Key Laboratory of Life-Organic Analysis, Key Laboratory of Pharmaceutical Intermediates and Analysis of Natural Medicine, College of Chemistry and Chemical Engineering, Qufu Normal University, Qufu, 273165, China

^b Institute of Functional Materials and Molecular Imaging, College of Clinical Medicine, Key Laboratory of Hainan Trauma and Disaster Rescue, College of Emergency and Trauma, Hainan Medical University, Haikou, 571199, China

^c Laboratory of Tibetan Medicine Research & Qinghai Key Laboratory of Qinghai-Tibet Plateau Biological Resources, Northwest Institute of Plateau Biology, Chinese Academy of Science, Xining, 810001, China

ARTICLE INFO

Keywords:

Fluorescent probe
Near-infrared fluorescence
Mitochondrial hydrazine
Imaging analysis

ABSTRACT

Hydrazine (N₂H₄) has been listed as a possible human carcinogen. It can cause severe damage to various organs through respiratory tract, skin and digestive tract. Although some fluorescent probes have been developed for imaging of N₂H₄, there is very few entry of application *in vivo*, probably limited by the short fluorescence emission wavelengths. Moreover, the sensitivity also needs to be improved to meet the requirement of detection *in vivo*. Hence, we design and synthesize a new NIR ratiometric fluorescent probe Cy-OAc based on cyanine derivatives for the sensitive detection of N₂H₄ in cells and in mice models. Cy-OAc consists of a large π -conjugated system and a masking unit for both regulating the π -system and tracing N₂H₄. Cy-OAc holds the emission profile centered at 825 nm under the excitation of 730 nm, and upon reaction with N₂H₄, it shifts the emission profile centered at 662 nm with an excitation at 540 nm, resulting in the NIR ratiometric emission response, as well as a distinct color change that can be distinguished by the naked eye. Cy-OAc has been successfully applied to imaging the N₂H₄ in apoptotic cells. The results reveal that N₂H₄ can lead to the apoptosis of HeLa cells *via* the damage of mitochondrial membrane potential. Taking advantage of the NIR emissions, Cy-OAc exhibits the deep tissue penetration of 700 μ m in kidney tissue. Our probe Cy-OAc is further utilized to visually detect N₂H₄-metabolism and estimate kidney damage in mice models. We envision that the probe Cy-OAc can be an attractive chemical tool for exploring N₂H₄ in bio-specimen.

1. Introduction

Hydrazine (N₂H₄) is widely used in rocket propulsion fuel for its flammable and explosive characteristics. Because of its versatile chemical properties, it is also an important chemical material in many industrial fields such as chemistry, medicine and agriculture [1]. However, N₂H₄ has considerable toxic effects on human health and can cause serious environmental pollution during its manufacture, usage, transportation and disposal [2]. N₂H₄ can volatilize in air or dissolve in water, therefore, can easily enter human body through diet or inhalation, resulting in serious damage to organs and nervous system, such as respiratory tract infection, liver and kidney damage, carcinogenic, as well as teratogenic and mutagenic effects [3–5]. The damage of N₂H₄ to the nervous system is related to the decrease of inhibitory neurotransmitter γ -aminobutyric acid and its receptor, the increase of

excitatory amino acids, and the dysfunction of energy metabolism. After poisoning, the electroencephalogram (EEG) with tonic clonic convulsion accompanied by epileptic seizures will occur. Inhalation of high concentrations of N₂H₄ will cause throat itching, cough, chest urgency, dyspnea, severe laryngitis, pulmonary edema. As a result of the harmful effects of N₂H₄ on human health, it has been classified as a potential human carcinogen, and its threshold value in drinking water is restricted below 10 ppb [6]. Therefore, it is important to develop reliable methods with high sensitivity and selectivity for the detection of trace N₂H₄ in environmental and biological samples.

Traditional analytical techniques including high performance liquid chromatography, gas chromatography, electrochemical analysis and colorimetric method have been developed and applied to the evaluation of N₂H₄ in environmental samples [7–10]. However, these techniques are not suitable for the *in situ* detection of N₂H₄ in living bio-specimens.

* Corresponding authors at: The Key Laboratory of Life-Organic Analysis, Key Laboratory of Pharmaceutical Intermediates and Analysis of Natural Medicine, College of Chemistry and Chemical Engineering, Qufu Normal University, Qufu, 273165, China.

E-mail addresses: chenandguang@163.com (G. Chen), jmyou6304@163.com (J. You), fbyu@yic.ac.cn (F. Yu).

<https://doi.org/10.1016/j.snb.2019.01.116>

Received 11 December 2018; Received in revised form 22 January 2019; Accepted 24 January 2019

Available online 24 January 2019

0925-4005/ © 2019 Elsevier B.V. All rights reserved.

Fluorescent bioimaging technology coupled with small molecule fluorescent probe has become a powerful tool for the detection of trace biologically reactive species owing to its advantages in high temporal resolution, non-invasiveness, and good bio-compatibility in real time and *in situ* [11–16]. In recent years, many fluorescent probes have been developed for N_2H_4 detection based on various chemical strategies [17–28]. Although most of these fluorescent probes have been used for imaging of N_2H_4 in cells, fewer of them were applied for *in vivo* imaging. Compared with the imaging of N_2H_4 in cells, visualizing of N_2H_4 in tissues or *in vivo* can directly provide the toxicant physiological distribution in the long term dynamic processes, instead of in a short time or in an intracellular local range. The detection of N_2H_4 *in vivo* is often hindered in the visible region because of the limited penetration depth in tissues. Near-infrared (NIR) probes have attracted considerable interests due to their advantages of reduced tissue absorption, deeper tissue penetration, minimal light damage, and low background interference [29–31]. However, the fluorescence signal acquiring from a single probe may be interfered by the concentration-independent experimental or physiological factors, such as intracellular uneven delivery and distribution, different permeability and retention in tissues, instrument error from light source stability [32]. These factors may result in an increase in false probability. Ratiometric probes can offer self-calibration for signal correction by employing the ratio of the emission intensity at two different wavelengths, which is satisfactory enough for the urgent requirement of biological analysis, especially a NIR ratiometric probe which works with the two NIR emissions at different wavelengths [33–35]. Moreover, the sensitivity is also crucial to improve the ratio of signal to noise in living cells and *in vivo*.

Herein, we proposed a new fluorescent probe Cy-OAc for N_2H_4 detection in cells, in tissue, and in mice (Scheme 1). The ethyl ester bond in the probe Cy-OAc was the reaction site for selectively capturing N_2H_4 . In the presence of N_2H_4 , the ester was broken, and the rearrangement of the extended π -system across the probe molecule led to a change in emission profiles from 825 nm to 662 nm. The limit of detection was 0.48 ppb. We applied the probe Cy-OAc for ratiometric imaging analysis of N_2H_4 in cells, kidney tissue, and living mice. We also evaluated cell apoptosis induced by different concentrations of N_2H_4 . Moreover, benefiting from the ratiometric NIR response, we examined the N_2H_4 metabolism and the injury to kidney in living mice.

2. Experimental

2.1. Synthesis of probe Cy-OAc

The compounds were synthesized according to the general procedure in Scheme 1. Keto-Cy (0.118 g, 0.2 mmol) and triethylamine (0.277 mL, 2 mmol, 10 equivalents) were dissolved in 5.0 mL anhydrous CH_2Cl_2 for 3 min under the condition of Ar at 0 °C. Then, acetyl chloride (0.141 mL, 2 mmol, 10 equivalents in 5.0 mL of CH_2Cl_2) was added dropwise to the solution. The mixture was stirred at room temperature for 5 h. The color of the solution changed from red to green. TLC was used to monitor the reaction until the raw material was completely consumed. After removing the organic phase under a vacuum, the crude

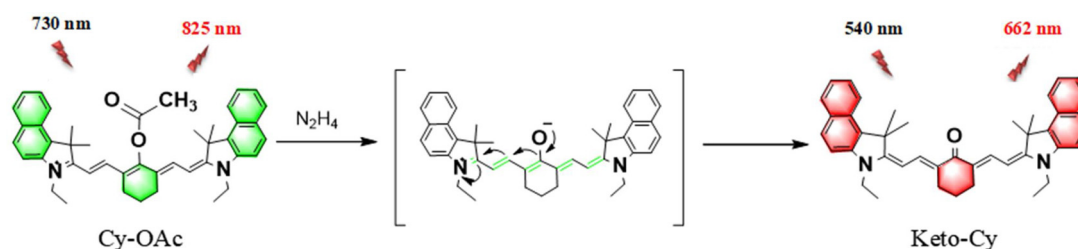
product was purified by column chromatography (EtOAc/MeOH from 100/1 to 4/1) to obtain the probe Cy-OAc, as a dark green solid (0.110 g, 72%). 1H NMR (500 MHz, $CDCl_3-d_1$) δ (ppm): 8.14–8.12 (t, 2 H), 7.99–7.96 (t, 4 H), 7.94 (d, 1 H), 7.83–7.80 (d, 2 H), 7.65–7.62 (m, 4 H), 7.48–7.37 (t, 3 H), 6.20–6.16 (d, 2 H), 4.36–4.32 (s, 4 H), 2.74–2.72 (s, 2 H), 2.19 (s, 3 H), 1.96 (s, 12 H), 1.54–1.42 (m, 8 H). ^{13}C NMR (125 MHz, $CDCl_3-d_1$) δ (ppm): 173.86, 172.71, 168.27, 159.58, 140.50, 139.52, 139.42, 133.92, 132.16, 131.16, 130.39, 129.16, 128.33, 128.06, 125.55, 125.36, 125.02, 122.43, 122.25, 111.07, 110.83, 110.39, 100.06, 99.51, 51.40, 51.11, 49.34, 40.14, 28.46, 28.39, 27.97, 24.71, 21.14, 21.00, 12.89. LC-MS (ESI⁺): m/z [$C_{44}H_{47}N_2O_2$]⁺; calcd, 635.3632; found [M]⁺: 635.3632.

2.2. The experiments in cell models

To test the robustness of the applicability of probe Cy-OAc, we used two types of cells human hepatocellular carcinoma cell line (SMMC-7721) and human hepatocellular liver carcinoma cell line (HepG2). The cells were respectively inoculated on 25-petri dishes and adhered for 24 h and treated with different concentrations of N_2H_4 (0 μ M, 20 μ M, 40 μ M, 60 μ M, 80 μ M and 100 μ M) for 20 min, respectively. Then the cells were washed with the fresh completion medium for three times to remove surplus N_2H_4 . Before imaging, the cells were incubated with the probe Cy-OAc (5 μ M) for 60 min. The imaging analysis was performed through confocal laser scanning microscope. The fluorescence was collected at channel 1 and channel 2, channel 1: 800–850 nm (λ_{ex} = 730 nm), channel 2: 625–725 nm (λ_{ex} = 559 nm). For the apoptosis study, we used the N_2H_4 to incubate the human cervical cancer cells (HeLa). HeLa cells were loaded with N_2H_4 (0 mM, 0.4 mM, 0.8 mM, 1.2 mM, 1.6 mM and 2 mM) for 20 min, then incubated with 50 μ M Cy-OAc for 60 min after removing surplus N_2H_4 . For the apoptosis control, HeLa cells pretreated with probe (50 μ M) were incubated by the media containing NaClO (1 mM) for 1 h. The cells were followed by a LTE confocal laser scanning microscope (Olympus FV1000 confocal laser-scanning microscope) to report the homeostasis of mitochondrial N_2H_4 with an objective lens ($\times 40/60$). Flow cytometry data were collected by BD Biosciences FACS Aria. Annexin V-FITC (fluorescein isothiocyanate) and PI (propidium iodide) were used to indicate the different population of cells during apoptosis analysis. To follow the change of mitochondrial membrane potential, HeLa cells was incubated with JC-1 staining working solution (100 μ L JC-1 in 16 mL H_2O and 4 mL staining buffer) in absence or presence of N_2H_4 (1 mM) for 3 h. The resultant cells were analyzed with the confocal laser scanning microscope with excitation wavelengths set as 515 nm and 488 nm and collection wavelengths set as 600–700 nm and 500–600 nm, respectively.

2.3. Imaging of N_2H_4 in poisoning mice

Nude mouse (SPF/female, 4 weeks) were obtained from Hainan Medical University and all animal experiments were carried out in accordance with regulations. The PerkinElmer IVIS Lumina XR Series III system was used for imaging *in vivo*. The probe Cy-OAc (25 μ L, 50 μ M in



Scheme 1. The ratiometric fluorescent probe Cy-OAc for N_2H_4 and the sensing mechanism (For interpretation of the references to colour in this scheme text, the reader is referred to the web version of this article).

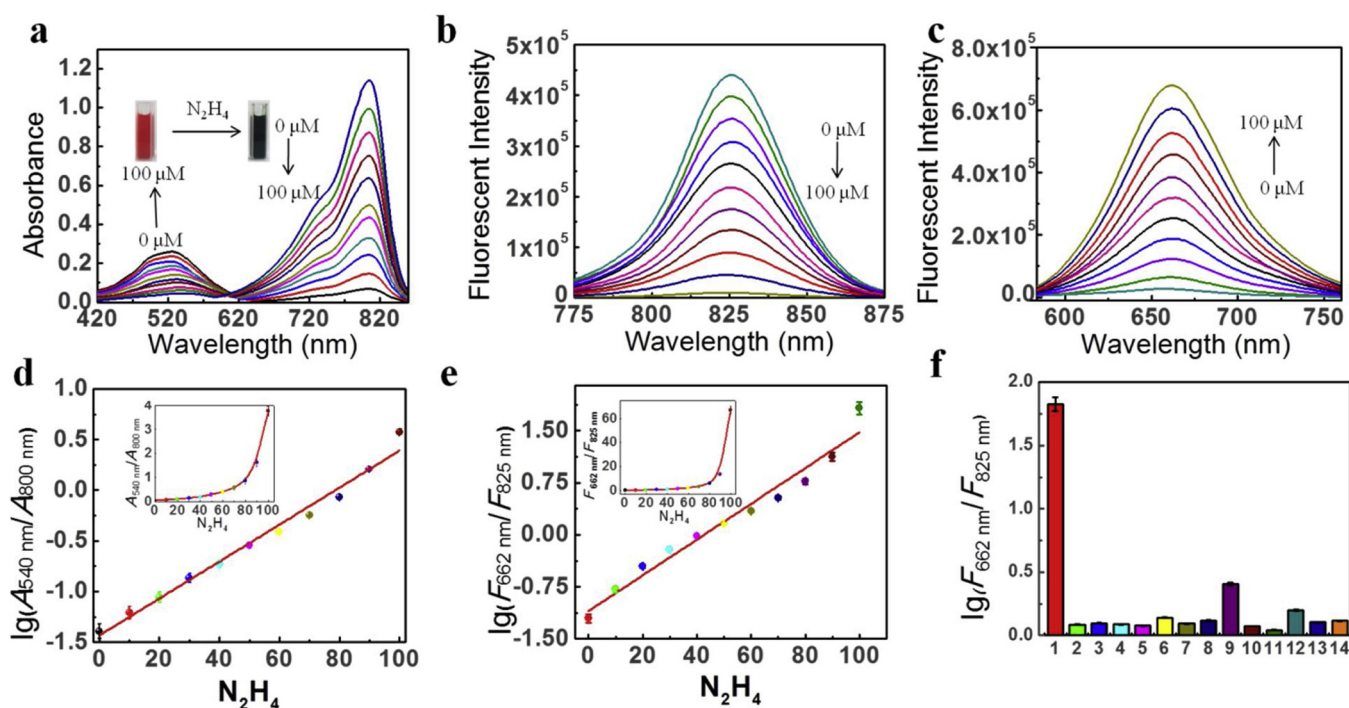


Fig. 1. Spectral properties and selectivity of Cy-OAc. Cy-OAc (5 μM) was incubated with increasing concentration of N_2H_4 (0–100 μM) at 37 $^\circ\text{C}$ in HEPES (pH 7.4, 10 mM). (a) Dose-dependent absorbance spectra of Cy-OAc towards N_2H_4 . Inset: the color change before and after the reaction of Cy-OAc with N_2H_4 . The spectra were recorded after for 60 min. (b) Emission spectra of Cy-OAc towards N_2H_4 ($\lambda_{\text{ex}} = 730 \text{ nm}$). (c) Emission spectra of Cy-OAc towards N_2H_4 ($\lambda_{\text{ex}} = 540 \text{ nm}$). (d) The linear relationship between $\text{Lg}(A_{540 \text{ nm}}/A_{800 \text{ nm}})$ and N_2H_4 . Inset: Ratio signals ($A_{540 \text{ nm}}/A_{800 \text{ nm}}$) of Cy-OAc towards N_2H_4 . (e) The linear relationship between $\text{Lg}(F_{662 \text{ nm}}/F_{825 \text{ nm}})$ and N_2H_4 . Inset: Ratio signals ($F_{662 \text{ nm}}/F_{825 \text{ nm}}$) of Cy-OAc towards N_2H_4 . (f) fluorescent ratio $\text{Lg}(F_{662 \text{ nm}}/F_{825 \text{ nm}})$ to various reactive species: 1, 100 μM hydrazine; 2, 1 mM cysteine; 3, 1 mM homocysteine; 4, 1 mM lysine; 5, 1 mM glutamine; 6, 1 mM glutathione; 7, 1 mM methylamine; 8, 1 mM n-butylamine; 9, 1 mM hydroxylamine; 10, 1 mM ethylenediamine; 11, 1 mM ammonia; 12, 1 mM triethylamine; 13, 1 mM urea; 14, 1 mM thiourea. All data were acquired in HEPES buffer (pH 7.4, 10 mM) at 37 $^\circ\text{C}$ for 60 min. $F_{662 \text{ nm}}$: $\lambda_{\text{ex}} = 540 \text{ nm}$, $\lambda_{\text{em}} = 662 \text{ nm}$; $F_{825 \text{ nm}}$: $\lambda_{\text{ex}} = 730 \text{ nm}$, $\lambda_{\text{em}} = 825 \text{ nm}$ (For interpretation of the references to colour in this figure text, the reader is referred to the web version of this article).

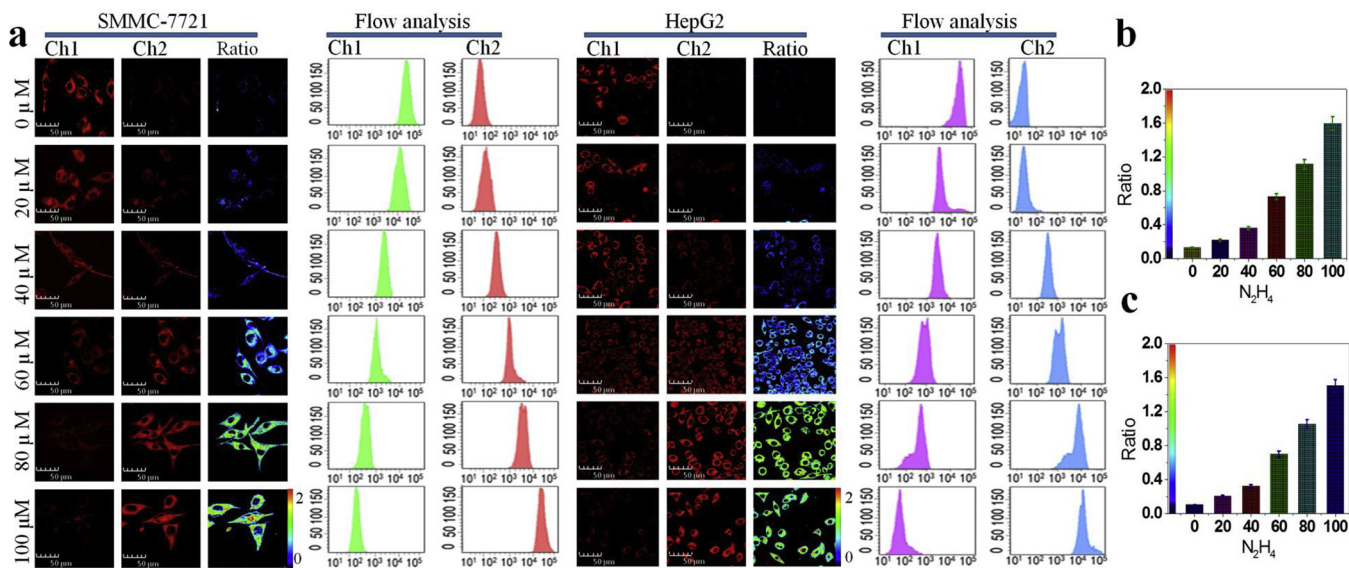


Fig. 2. Quantitative analysis of N_2H_4 fluctuation in living cells by confocal imaging and flow cytometry analysis. (a) SMMC-7721 cells and HepG2 cells were loaded with 5 μM Cy-OAc and various concentrations of N_2H_4 (0 μM , 20 μM , 40 μM , 60 μM , 80 μM and 100 μM) for 60 min. Pseudo-color ratio images indicate the ratio of channel 2 vs channel 1 at corresponding concentrations. The fluorescence was collected at channel 1:800–850 nm ($\lambda_{\text{ex}} = 730 \text{ nm}$), channel 2: 625–725 nm ($\lambda_{\text{ex}} = 559 \text{ nm}$). Scale bar is 50 μm . Quantitative application of Cy-OAc by flow cytometry analysis. (b) The relationship between average fluorescence intensity and added various N_2H_4 concentrations of SMMC-7721 cells correspondingly in (a). (c) The relationship between average fluorescence intensity and added various N_2H_4 concentrations of HepG2 cells correspondingly in (a).

DMSO/saline: 1/9, v/v) were injected intraperitoneally into the mice. After 1 h, the N_2H_4 (25 μL , 500 μM in DMSO/saline: 1/9, v/v) was injected intraperitoneally. As the control, mice were injected

intraperitoneally with 200 μL of saline (0.9%) 12 h after fasting. Imaging analysis was taken after 0, 0.5, 1, 1.5 and 2 h of injection respectively. Isoflurane was used as an anesthetic in the whole process.

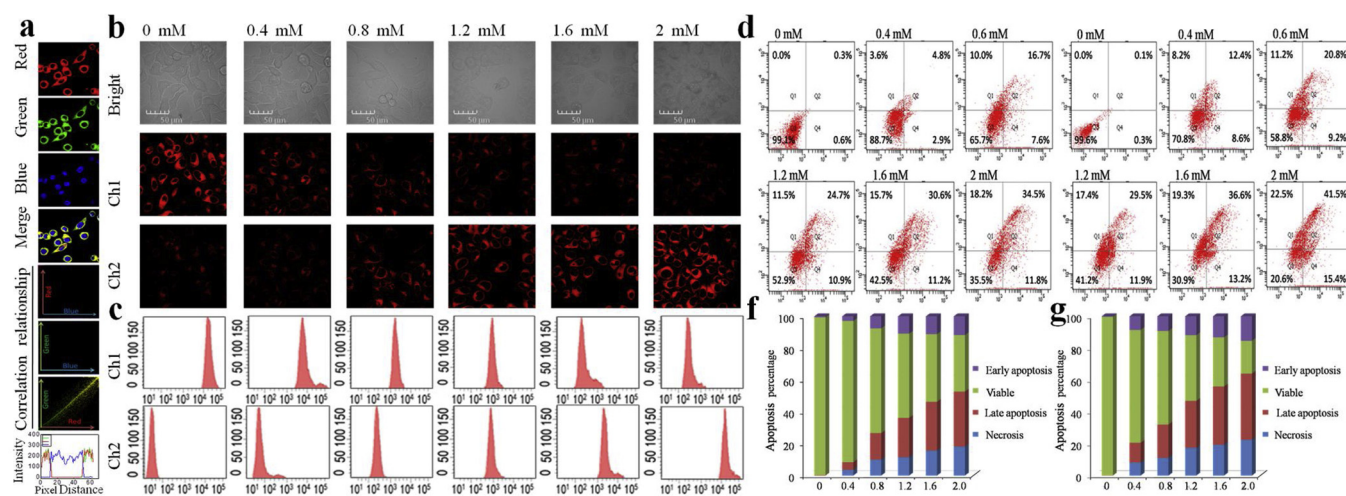


Fig. 3. (a) Mitochondrial multicolor colocalization in HeLa cells with probe Cy-OAc, rhodamine 123, and Hoechst 33342. The cells were incubated with 5 mM Cy-OAc for 20 min (Red), 1 mg/mL rhodamine 123 for 15 min (Green), and 1 mg/mL Hoechst 33342 for 30 min (Blue). Fluorescence images collection windows: from 800 to 850 nm for (Red), from 550 to 600 nm for (Green), and from 440 to 500 nm for (Blue), $\lambda_{\text{ex}} = 730$ nm, 515 nm, and 405 nm, respectively. Merged red, green, and blue channels (Merge). (Correlation Relationship) Displayed the colocalization and correlation between two selected channels form (Merge): red, green and blue and intensity profile of regions of interest (red arrow in Merge). (b) HeLa cells loaded with 50 μM Cy-OAc and 0 mM, 0.4 mM, 0.8 mM, 1.2 mM, 1.6 mM and 2 mM N₂H₄ for 60 min. The fluorescence was collected at channel 1 and channel 2, channel 1: 800–850 nm ($\lambda_{\text{ex}} = 730$ nm), channel 2: 625–725 nm ($\lambda_{\text{ex}} = 559$ nm). Scale bar is 10 μm . (c) Flow cytometry analysis for quantitative application of Cy-OAc. (d) Apoptosis and necrosis analysis of HeLa cells incubated with various concentrations of N₂H₄. (e) Apoptosis and necrosis analysis of HeLa cells incubated with NaClO. Q1): necrosis, Q2): late apoptosis, Q3): viable, Q4): early apoptosis. (f), (g) Apoptosis analysis were the distribution diagrams for (d) and (e), respectively (For interpretation of the references to colour in this figure legend, the reader is referred to the web version of this article).

The fluorescent images were collected from two fluorescence collection windows, channel 1: $\lambda_{\text{ex}} = 730$ nm with filter 820 ± 20 nm, and channel 2: $\lambda_{\text{ex}} = 540$ nm with filter 660 ± 20 nm. The mice were anesthetized by intraperitoneal injection of chloral hydrate (4%; 3 mL/kg) and vivisected to expose kidney. Saline (0.9%) was used to wash blood off. Masson Staining: Kidneys were harvested from mice and were excised. The tissues were embedded in paraffin after being fixed with formaldehyde (10%). The treated kidneys were cut and dewaxed. Then the slices were dehydrated with graded ethanol series and were washed with distilled water. The kidneys slices were stained with Masson's trichrome for observation. All experimental procedures were conducted in conformity with institutional guidelines for the care and use of laboratory animals, and protocols were approved by the Institutional Animal Care and Use Committee in Hainan Medical University, Haikou, China.

3. Results and discussion

3.1. The detection mechanism of Cy-OAc

To construct a NIR ratiometric fluorescent probe for the detection of N₂H₄, our strategy relies on the modulation of the conjugated polymethine π -electron system of a NIR heptamethine cyanine derivative (Keto-Cy). The derivatives of cyanine dye offer the NIR emission profile, high extinction coefficient, low biological toxicity, good biocompatibility, and the octanol/water partition coefficient [36,37]. As for the recognition moiety towards N₂H₄, we select the hydrazinolysis reaction of acetate ester [38]. As shown in Scheme 1, the fluorescence regulation mechanism relies on internal charge transfer (ICT) process. After masking the acetate group into the meso-oxygen atom of Keto-Cy, the long π -conjugated chain between two nitrogen atoms formed, allowing for the longer NIR emission wavelength of the probe Cy-OAc. The reaction with N₂H₄ resulted in the ketone form of Keto-Cy following the blue shift in emission profile, thereby exhibiting the capability of ratiometric response towards N₂H₄.

3.2. Spectroscopic properties of probe Cy-OAc toward N₂H₄

The properties of probe Cy-OAc toward N₂H₄ were measured under simulated physiological conditions (10 mM HEPES, pH 7.4). As shown in Fig. 1a, the free probe displayed the maximum absorption wavelength at 800 nm. Upon the addition of N₂H₄, the maximum absorption wavelength blue-shifted to 540 nm and the color changed from green to red, indicating that Cy-OAc could act as a "naked eye" colorimetric indicator for N₂H₄ detection. UV titration results demonstrated that there was an excellent linear relationship between the absorbance ratio ($A_{540 \text{ nm}}/A_{800 \text{ nm}}$) and the concentration of N₂H₄ (0–80 μM), the standard curve was $A_{540 \text{ nm}}/A_{800 \text{ nm}} = 0.009 \times [\text{N}_2\text{H}_4] \mu\text{M} - 0.078$, with $r = 0.9247$ (Fig. 1d). Fluorescence tests illustrated that the probe Cy-OAc possessed the NIR emission spectra centered at 825 nm. Upon the gradual addition of N₂H₄, the fluorescence signal at 825 nm decreased, meanwhile a new emission centered at 662 nm increased (Fig. 1b and c). The linear relationship of the probe Cy-OAc towards the concentrations of N₂H₄ (0–80 μM) was achieved, the calibration curve was $F_{662 \text{ nm}}/F_{825 \text{ nm}} = 0.062 \times [\text{N}_2\text{H}_4] \mu\text{M} - 0.828$, with $r = 0.8955$ (Fig. 1e). Under the experimental conditions, the detection limit was determined to be 0.48 ppb, which is lower than that of the current fluorescent probes [39–43], and also was much lower than the threshold value in drinking water (10 ppb). The selectivity experiments were performed in Fig. 1f. The results showed that neither the high amounts of amine compounds (such as cysteine, homocysteine, lysine, glutamine, glutathione, methylamine, n-butylamine, hydroxylamine, ethylenediamine, ammonia, triethylamine, urea, thiourea) nor the common anion and cation (Na^+ , Ca^{2+} , Mg^{2+} , Cd^{2+} , Pb^{2+} , Ni^{2+} , Cu^{2+} , Al^{3+} , Co^{3+} , HPO_4^{2-} , ClO_4^- , CO_3^{2-} , Cl^-) could cause the interferences (Fig. S6). Therefore, the probe Cy-OAc was rationally designed and proved to be a sensitive NIR ratiometric fluorescent probe for the selective detection of N₂H₄.

3.3. Imaging of N₂H₄ in cells with the probe Cy-OAc

Before the intracellular application of our probe, the cytotoxicity test for Cy-OAc was performed via MTT assay using standard cell

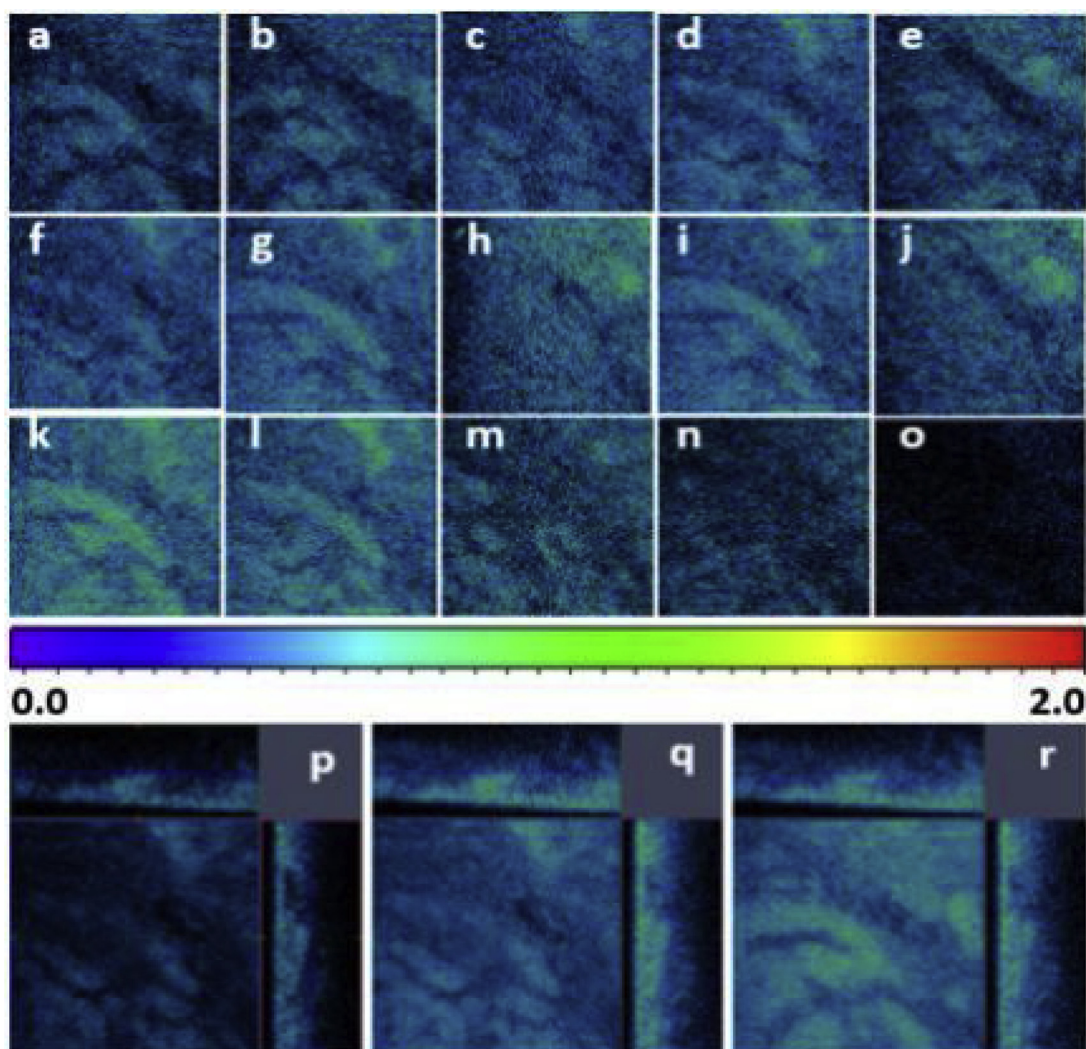


Fig. 4. The ratiometric images on the basis of fluorescent ratios between channel 1 (800–850 nm) and channel 2 (625–725 nm) at different depths (a–o: 570–710 μm with increment of 10 μm ; p–r: 3D scanning images for a, g and k, respectively) of kidney tissue of mouse incubated with hydrazine (500 μM) and then Cy-OAc (50 μM).

viability protocols. Various concentrations of our probe Cy-OAc (0, 10, 20, 30, 40, 50, 60, 70, 80 μM) were incubated with three cell lines (SMMC-7721, HepG2 and HeLa cells) for 24 h. As shown in Fig. S7, the cell viabilities were still over 90% even the probe concentration was as high as 80 μM . These results indicated that the probe Cy-OAc held a good biocompatibility to living cells.

To test the biological applicability of this probe, we performed the intracellular imaging of N_2H_4 in SMMC-7721 and HepG2 cells. As illustrated in Fig. 2, the two cell lines were treated with different concentrations of N_2H_4 (0 μM , 20 μM , 40 μM , 60 μM , 80 μM and 100 μM) for 20 min, respectively. Then the cells were washed with the fresh completion medium for three times to remove surplus N_2H_4 . Before imaging, the cells were incubated with the probe Cy-OAc (5 μM) for 60 min. The imaging analysis was performed through confocal laser scanning microscope. The control cell lines (0 μM N_2H_4) emitted strong fluorescence in channel 1 (800–850 nm) and faint fluorescence in channel 2 (625–725 nm), indicating no N_2H_4 in cells. After the incubation with the increasing concentrations of N_2H_4 , there observed the gradually enhanced fluorescence in the channel 2, accompanied by a fluorescence decrease in the channel 1. Correspondingly, the ratio images provided the increased fluorescence ratios, which reconstructed from the two channels ($\text{Ratio} = F_{625-725 \text{ nm}}/F_{800-850 \text{ nm}}$). These results demonstrated that the probe Cy-OAc could be utilized to detect the changes of N_2H_4 in cells. To further confirm this issue, we performed

flow cytometry analysis for quantifying the intracellular fluorescence changes in large population of cells. As shown in Fig. 2, there were clear peak shift toward the region of weak intensity in channel 1 and meanwhile the peak shift toward the strong intensity region in channel 2, which was consistent with the results recorded by confocal fluorescence microscopy. The above experiments demonstrated that our probe Cy-OAc could detect intracellular N_2H_4 with its NIR ratiometric fluorescence response.

3.4. Evaluation of mitochondrial N_2H_4 cytotoxicity

Mitochondria are considered as the important organelles in cells, which are involved in a wide variety of essential physiological processes, including cellular metabolism, cell signaling, and cell apoptosis. Mitochondrial dysfunctions are associated with cancer, as well as several neurological and cardiovascular diseases. Then we preliminarily evaluated N_2H_4 cytotoxicity in mitochondria. The probe Cy-OAc had iminiumcation which could target and accumulate in mitochondria [44]. The multicolor colocalization analysis of the dyads based on the simultaneous acquisition of spectrally separated images could measure molecular distances with accuracy better than 10 nm [31]. We employed the co-localization assay to verify Cy-OAc functioned in mitochondria. The HeLa cells were contaminated with the probe Cy-OAc for 20 min, a commercial mitochondrial dye rhodamine 123 for 15 min,

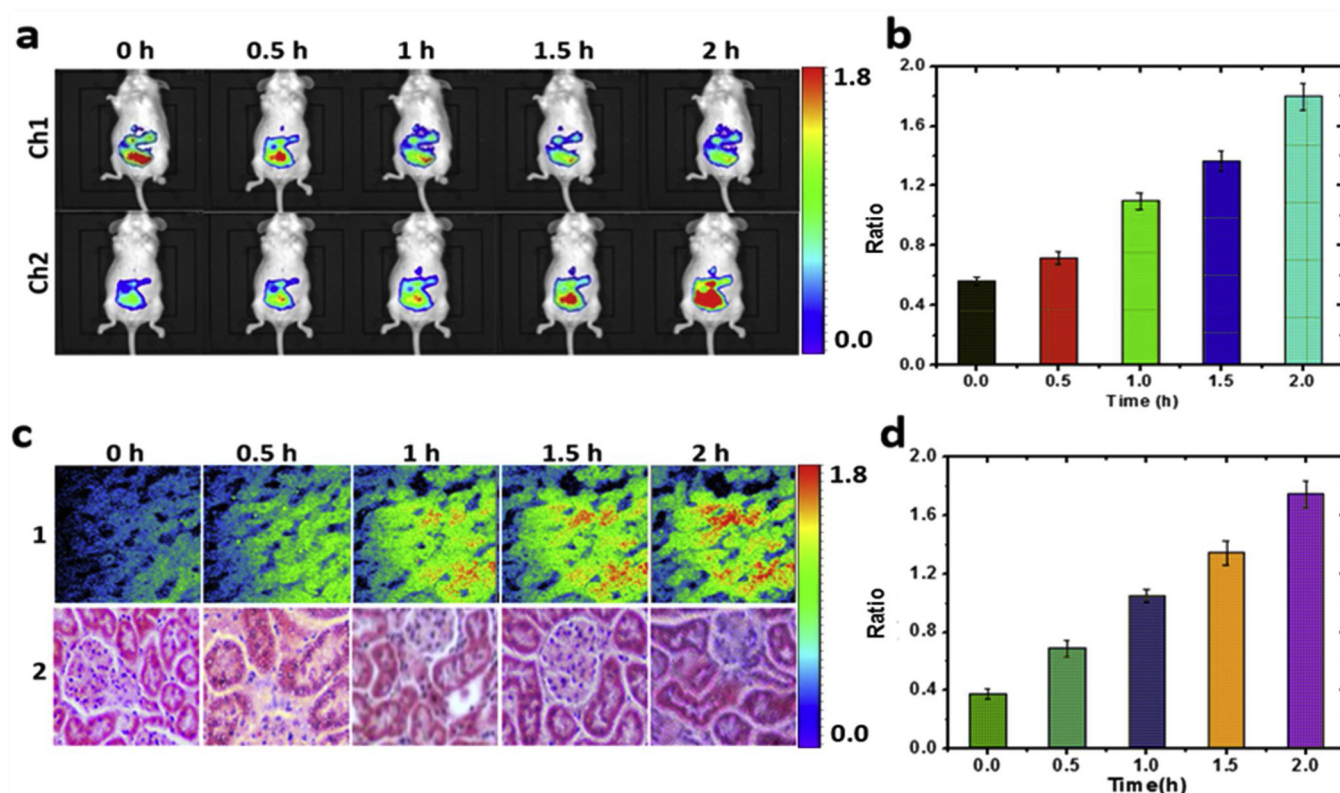


Fig. 5. (a) Fluorescence images of mouse by intraperitoneal injection of Cy-OAc (25 μ L, 50 μ M in DMSO/saline: 1/9, v/v) and then N_2H_4 (25 μ L, 500 μ M in DMSO/saline: 1/9, v/v). (b) Fluorescence intensity ratio of channel 1 and channel 2 at different times (F_{ch2}/F_{ch1}) from (a). (c) The kidney tissue imaging (1) and the Masson's trichrome stain of the kidney tissue (2). (d) Fluorescence intensity ratio (F_{ch2}/F_{ch1}) from the tissue imaging in (c). The fluorescent images were collected from two fluorescence collection windows, channel 1: λ_{ex} = 730 nm with filter 820 ± 20 nm, and channel 2: λ_{ex} = 540 nm with filter 660 ± 20 nm.

and a nuclear fluorescent marker Hoechst 33342 for 30 min. The fluorescence images acquired from the three channels (red, green, and blue channels) and the merged image from the three channels was shown in Fig. 3a. As illustrated in Fig. 3a, there was almost no correlation between the probe Cy-OAc and Hoechst 33342, and the rhodamine 123 also showed low correlation with Hoechst 33342. While the fluorescence between Cy-OAc and rhodamine 123 exhibited excellent overlap with a high Pearson's coefficient $R = 0.99$. These results suggested that the probe Cy-OAc could locate in mitochondria and potentially detect N_2H_4 in mitochondria.

We next set out to investigate cell apoptosis induced by N_2H_4 in HeLa cells. As displayed in Fig. 3b, HeLa cells were pretreated with hydrazine (0–2 mM) for 20 min, washed with the fresh cell culture medium, then incubated with probe Cy-OAc (5 μ M) for 60 min. The control showed the strong fluorescence in channel 1 (800–850 nm) and weak fluorescence in channel 2 (625–725 nm). Upon the addition of the increasing N_2H_4 concentration, the fluorescence intensity in channel 1 progressively decreased, and the fluorescence intensity in channel 2 gradually increased, indicating that the raise level of N_2H_4 in cells. These fluorescence images were further validated via flow cytometric analysis (Fig. 3c). The basic apoptosis of the cell in control was very low, and the cell had good proliferation and cell morphology. With the increasing concentration of N_2H_4 , cell apoptosis increased and cell morphology became shrank. We hypothesized that the increased N_2H_4 accumulation in mitochondria contributed to the aggravation of cells apoptosis. Cell apoptosis always accompanied by the collapse of mitochondrial membrane potential, next we added the exogenous hydrazine, which destroyed the membrane potential and thus causing cell apoptosis [45]. For confirming this result, we tested mitochondrial membrane potential by incubating the cells with a membrane potential dye JC-1 in the absence or presence of hydrazine (Fig. S10). The green

fluorescence indicated the collapse of membrane potential, which confirmed that the unregulated apoptosis was associated with the cytotoxicity of hydrazine. We also imposed artificial intervention of late apoptosis to cells by adding the NaClO which could serve as the inducer for apoptosis [46]. Fig. 3d and e dimpled the remarkable aggravation of apoptosis, demonstrating that the elevated level of apoptotic cells was caused by the mitochondrial variation. The change of membrane potential was shown in Fig. S11. Therefore, the above experiments demonstrated that our probe Cy-OAc was an effective chemical tool for the detection of N_2H_4 in mitochondria.

3.5. Imaging of hydrazine metabolism in mice

Before the practical application *in vivo*, we test the penetrating capability of probe in tissue. The kidney tissue slice (thickness 2 mm) of mice was fully infiltrated hydrazine (500 μ M) for 20 min, washed the fresh slice with saline three times, then incubated with Cy-OAc (50 μ M) for 1 h before imaging. As shown in Fig. 4, owing to the NIR fluorescent emission, the imaging depth of this probe could reach to 700 μ m, demonstrating that this probe possessed the satisfactory applicability for imaging analysis *in vivo*. For further exploring the injury to kidney tissue, the excellent optical properties of probe Cy-OAc facilitated us to perform the metabolic monitoring of N_2H_4 in mice (Fig. 5). The probe Cy-OAc (25 μ L, 50 μ M in DMSO/saline: 1/9, v/v) was intraperitoneally injected into the mice [47,48]. After 1 h, the N_2H_4 (25 μ L, 500 μ M in DMSO/saline: 1/9, v/v) was intraperitoneally injected again. The mice were continuously maintained for 0, 0.5, 1, 1.5 and 2 h for fluorescence imaging of N_2H_4 *in vivo*, then sacrificed and isolated kidney for fluorescence image analysis. As shown in Fig. 5a, the channel 1 and channel 2 presented the strong and weak fluorescence signal respectively when no N_2H_4 was injected. After the injection of N_2H_4 , the fluorescence

intensity in channel 1 decreased and meanwhile the intensity in channel 2 began to increase. During the 2 h after injection, the fluorescence images demonstrated that the fluorescence ratio of (F_{ch2}/F_{ch1}) gradually increased, which indicated that the N_2H_4 in tissue was increased with the metabolism of mouse. Since N_2H_4 could cause the apoptotic injury to cells, we reasoned that the increased level of hydrazine would lead to the tissue injury to the kidney of the mice. Accordingly, we harvested kidney tissue of the parallel group and performed both the fluorescence imaging and Masson's trichrome stain analysis. As shown in Fig. 5c, the fluorescence ratio (F_{ch2}/F_{ch1}) increased from 0 to 2 h. The Masson's trichrome stain illustrated that the collagenous fibers were normal without the injection of N_2H_4 . The glomerulus exhibited integral and clear profile, and the nuclei were regular. While the mice with the injection of N_2H_4 , the tissue showed gradually increased collagenous fiber, and also the glomerulus exhibited borderless profile, which could be attributed to the injury of the increased hydrazine. The fluorescence changes in Fig. 5a and c were quantified in Fig. 5b and d. Our probe Cy-OAc was proved to be an effective tool to real-time visualized hydrazine in living mice.

4. Conclusions

In summary, we have developed a highly sensitive NIR fluorescent probe Cy-OAc for imaging of N_2H_4 in cells and in mice models. The flexible regulation of π -conjugated system enabled the probe Cy-OAc to release two NIR-emission before and after the reaction with N_2H_4 , resulting in the sensitive ratiometric fluorescence response to N_2H_4 detection in mitochondria of HeLa cells. The probe Cy-OAc has been successfully applied to imaging the N_2H_4 in apoptotic cells. The results indicate that the accumulation of N_2H_4 in mitochondria can lead to severe cell apoptosis. Benefiting from the NIR fluorescence emissions, the probe Cy-OAc exhibits the deep tissue penetration in mice. We employ the probe for imaging of N_2H_4 metabolism and visual inspecting the kidney tissue damage in mice models. These results highlight that our probe Cy-OAc can be used as a powerful chemical tool for N_2H_4 -associated detection *in vitro* and *in vivo*.

Competing financial interest

The authors declare no competing financial interest.

Acknowledgments

We thank the National Nature Science Foundation of China (Nos. 21775162 and 21864011), China Postdoctoral Science Foundation (Grant 2017M622254), Natural Science Foundation of Shandong Province (Grant ZR201709240033), Talent Program of Hainan Medical University (Grants XRC180006 and XRC180007), and Hundred-Talent Program (Hainan 2018).

Appendix A. Supplementary data

Supplementary material related to this article can be found, in the online version, at doi:<https://doi.org/10.1016/j.snb.2019.01.116>.

References

- [1] J. Zhao, Y. Xu, H. Li, A. Lu, S. Sun, A facile intracellular fluorescent probe for detection of hydrazine and its application, *New J. Chem.* 37 (2013) 3849–3852.
- [2] J. Fan, W. Sun, M. Hu, J. Cao, G. Cheng, H. Dong, K. Song, Y. Liu, S. Sun, X. Peng, An ICT-based ratiometric probe for hydrazine and its application in live cells, *Chem. Commun.* 48 (2012) 8117–8119.
- [3] G. Li, Y. Liu, J. Song, Y. Ye, A fluorescein-based colorimetric and fluorescent probe for hydrazine and its bioimaging in live cells, *J. Fluoresc.* 27 (2017) 323–329.
- [4] S. Garrod, M.E. Bollard, A.W. Nicholls, S.C. Connor, J. Connelly, J.K. Nicholson, E. Holmes, Integrated metabolomic analysis of the multiorgan effects of hydrazine toxicity in the rat, *Chem. Res. Toxicol.* 18 (2005) 115–122.
- [5] C.A. Reilly, S.D. Aust, Peroxidase substrates stimulate the oxidation of hydralazine to metabolites which cause single-strand breaks in DNA, *Chem. Res. Toxicol.* 10 (1997) 328–334.
- [6] A. Umar, M.M. Rahman, S.H. Kim, Y.B. Hahn, Zinc oxide nanonail based chemical sensor for hydrazine detection, *Chem. Commun.* 2 (2008) 166–168.
- [7] J. Zhang, Y. Zhou, J. Yoon, J.S. Kim, Recent progress in fluorescent and colorimetric chemosensors for detection of precious metal ions (silver, gold and platinum ions), *Chem. Soc. Rev.* 40 (2011) 3416–3429.
- [8] C. Batchelor-McAuley, C.E. Banks, A.O. Simm, T.G.J. Jones, R.G. Compton, The electroanalytical detection of hydrazine: a comparison of the use of palladium nanoparticles supported on boron-doped diamond and palladium plated BDD microdisc array, *Analyst* 131 (2006) 106–110.
- [9] M. Sun, L. Bai, D.Q. Liu, A generic approach for the determination of trace hydrazine in drug substances using in situ derivatization-headspace GC–MS, *J. Pharm. Biomed. Anal.* 49 (2009) 529–533.
- [10] T. Kawasaki, M. Maeda, A. Tsuji, Determination of plasma and urinary cortisol by high-performance liquid chromatography using fluorescence derivatization with dansyl hydrazine, *J. Chromatogr. Biomed. Appl.* 163 (1979) 143–150.
- [11] H. Kobayashi, M. Ogawa, R. Alford, P.L. Choyke, Y. Urano, New strategies for fluorescent probe design in medical diagnostic imaging, *Chem. Rev.* 110 (2010) 2620–2640.
- [12] X. Chen, X. Tian, I. Shin, J. Yoon, Fluorescent and luminescent probes for detection of reactive oxygen and nitrogen species, *Chem. Soc. Rev.* 40 (2011) 4783–4804.
- [13] M. Beija, C.A. Afonso, J.M. Martinho, Synthesis and applications of Rhodamine derivatives as fluorescent probes, *Chem. Soc. Rev.* 38 (2009) 2410–2433.
- [14] K. Dou, G. Chen, F. Yu, Y. Liu, L. Chen, Z. Cao, T. Chen, Y. Li, J. You, Bright sensitive ratiometric fluorescent probe enabling endogenous FA imaging and mechanistic exploration of indirect oxidative damage of FA in various living systems, *Chem. Sci.* 8 (2017) 7851–7861.
- [15] G.C.Vd. Bittner, E.A. Dubikovskaya, C.R. Bertozzi, C.J. Chang, In vivo imaging of hydrogen peroxide production in a murine tumor model with a chemoselective bioluminescent reporter, *Proc. Natl. Acad. Sci. U. S. A.* 107 (2010) 21316–21321.
- [16] G. Chen, F. Yu, R. Ren, Y. Liu, Z. Cao, G. Li, X. Zhao, L. Chen, H. Wang, J. You, Wide-acidity-range pH fluorescence probes for evaluation of acidification in mitochondria and digestive tract mucosa, *Anal. Chem.* 89 (2017) 8509–8516.
- [17] M.V.R. Raju, E.C. Prakash, H.C. Chang, H.C. Lin, A facile ratiometric fluorescent chemodosimeter for hydrazine based on Ing–Manske hydrazinolysis and its applications in living cells, *Dyes Pigm.* 103 (2014) 9–20.
- [18] S. Yu, S. Wang, H. Yu, Y. Feng, S. Zhang, M. Zhu, H. Yin, X. Meng, A ratiometric two-photon fluorescent probe for hydrazine and its applications, *Sens. Actuators B Chem.* 220 (2015) 1338–1345.
- [19] L. Cui, Z. Peng, C. Ji, J. Huang, D. Huang, J. Ma, S. Zhang, X. Qian, Y. Xu, Hydrazine detection in the gas state and aqueous solution based on the Gabriel mechanism and its imaging in living cells, *Chem. Commun.* 50 (2014) 1485–1487.
- [20] L. Xiao, J. Tu, S. Sun, Z. Pei, Y. Pei, Y. Pang, Y. Xu, A fluorescent probe for hydrazine and its in vivo applications, *RSC Adv.* 4 (2014) 41807–41811.
- [21] S.I. Reja, N. Gupta, V. Bhalla, D. Kaur, S. Arora, M. Kumar, A charge transfer based ratiometric fluorescent probe for detection of hydrazine in aqueous medium and living cells, *Sens. Actuators B Chem.* 222 (2016) 923–929.
- [22] Y. Tan, J. Yu, J. Gao, Y. Cui, Y. Yang, G. Qian, A new fluorescent and colorimetric probe for trace hydrazine with a wide detection range in aqueous solution, *Dyes Pigm.* 99 (2013) 966–971.
- [23] D. Zhou, Y. Wang, J. Jia, W. Yu, B. Qu, X. Li, X. Sun, H-Bonding and charging mediated aggregation and emission for fluorescence turn-on detection of hydrazine hydrate, *Chem. Commun.* 51 (2015) 10656–10659.
- [24] Z. Luo, B. Liu, T. Qin, K. Zhu, C. Zhao, C. Pan, L. Wang, Cyclization of chalcone enables ratiometric fluorescence determination of hydrazine with a high selectivity, *Sens. Actuators B Chem.* 263 (2018) 229–236.
- [25] Y. Sun, D. Zhao, S. Fan, L. Duan, A 4-hydroxynaphthalimide-derived ratiometric fluorescent probe for hydrazine and its in vivo applications, *Sens. Actuators B Chem.* 208 (2015) 512–517.
- [26] K. Tiensomjit, R. Noorat, S. Chomngam, K. Wechakorn, S. Prabpai, P. Kanjanasirirat, Y. Pewkliang, S. Borwornpinyo, P. Kongsaree, A chromogenic and fluorogenic rhodol-based chemosensor for hydrazine detection and its application in live cell bioimaging, *Spectrochim. Acta Part A* 195 (2018) 136–141.
- [27] W.D. Wang, Y. Hu, Q. Li, S.L. Hu, A carbazole-based turn-on fluorescent probe for the detection of hydrazine in aqueous solution, *Inorg. Chim. Acta* 477 (2018) 206–211.
- [28] Y. Qian, J. Lin, L. Han, L. Lin, H. Zhu, A resorufin-based colorimetric and fluorescent probe for live-cell monitoring of hydrazine, *Biosens. Bioelectron.* 58 (2014) 282–286.
- [29] B. Zhou, Y. Li, G. Niu, M. Lan, Q. Jia, Q. Liang, Near-infrared organic dye-based nano-agent for the photothermal therapy of cancer, *ACS Appl. Mater. Interfaces* 8 (2016) 29899–29905.
- [30] X. Zhao, Y. Li, D. Jin, Y. Xing, X. Yan, L. Chen, A near-infrared multifunctional fluorescent probe with an inherent tumor-targeting property for bioimaging, *Chem. Commun.* 51 (2015) 11721–11724.
- [31] H. Guo, G. Chen, M. Gao, R. Wang, Y. Liu, F. Yu, Imaging of endogenous hydrogen peroxide during the process of cell mitosis and mouse brain development with a near-infrared ratiometric fluorescent probe, *Anal. Chem.* 91 (2019) 1203–1210.
- [32] X. Huang, J. Song, B.C. Yung, X. Huang, Y. Xiong, X. Chen, Ratiometric optical nanoprobes enable accurate molecular detection and imaging, *Chem. Soc. Rev.* 47 (2018) 2873–2920.
- [33] K. Dou, G. Chen, F. Yu, Y. Liu, Z. Cao, G. Li, X. Zhao, L. Xia, L. Chen, H. Wang, J. You, A novel dual-ratiometric-response fluorescent probe for SO_2/ClO^- detection in cells and in vivo and its application in exploring the dichotomous role of SO_2 under the ClO^- induced oxidative stress, *Biomaterials* 133 (2017) 82–93.

- [34] L. Yuan, W. Lin, K. Zheng, L. He, W. Huang, ChemInform abstract: far-red to near infrared analyte-responsive fluorescent probes based on organic fluorophore platforms for fluorescence imaging, *Chem. Soc. Rev.* 42 (2013) 622–661.
- [35] K. Dou, G. Chen, F. Yu, Z. Sun, G. Li, X. Zhao, L. Chen, J. You, A two-photon ratiometric fluorescent probe for the synergistic detection of the mitochondrial SO₂/HClO crosstalk in cells and in vivo, *J. Mater. Chem. B* 5 (2017) 8389–8398.
- [36] X. Wang, J. Sun, W. Zhang, X. Ma, J. Lv, B. Tang, A near-infrared ratiometric fluorescent probe for rapid and highly sensitive imaging of endogenous hydrogen sulfide in living cells, *Chem. Sci.* 4 (2013) 2551–2556.
- [37] W. Sun, S. Guo, C. Hu, J. Fan, X. Peng, Recent development of chemosensors based on cyanine platforms, *Chem. Rev.* 116 (2016) 7768–7817.
- [38] B.R.N. Washburne, J.G. Miller, A.R. Day, The hydrazinolysis of methyl acetate, *J. Am. Chem. Soc.* 80 (1958) 5963–5965.
- [39] J. Zhang, L. Ning, J. Liu, J. Wang, B. Yu, X. Liu, X. Yao, Z. Zhang, H. Zhang, Naked-eye and near-infrared fluorescence probe for hydrazine and its applications in vitro and in vivo bioimaging, *Anal. Chem.* 87 (2015) 9101–9107.
- [40] B. Roy, S. Halder, A. Guha, S. Bandyopadhyay, Highly selective sub-ppm naked-eye detection of hydrazine with conjugated-1,3-diketo probes: imaging hydrazine in drosophila larvae, *Anal. Chem.* 89 (2017) 10625–10636.
- [41] F. Ali, H.A. Anila, N. Taye, D.G. Mogare, S. Chattopadhyay, A. Das, Specific receptor for hydrazine: mapping the in situ release of hydrazine in live cells and in an in vitro enzymatic assay, *Chem. Commun.* 52 (2016) 6166–6169.
- [42] L. Cui, C. Ji, Z. Peng, L. Zhong, C. Zhou, L. Yan, S. Qu, S. Zhang, C. Huang, X. Qian, Y. Xu, Unique tri-output optical probe for specific and ultrasensitive detection of hydrazine, *Anal. Chem.* 86 (2014) 4611–4617.
- [43] C. Hu, W. Sun, J. Cao, P. Gao, J. Wang, J. Fan, F. Song, S. Sun, X. Peng, A ratiometric near-infrared fluorescent probe for hydrazine and its in vivo applications, *Org. Lett.* 15 (2013) 4022–4025.
- [44] J. Zielonka, J. Joseph, A. Sikora, M. Hardy, O. Ouari, J. Vasquez-Vivar, G. Cheng, M. Lopez, B. Kalyanaraman, Mitochondria-targeted triphenylphosphonium-based compounds: syntheses, mechanisms of action, and therapeutic and diagnostic applications, *Chem. Rev.* 117 (2017) 10043–10120.
- [45] G. Chen, W. Zhou, C. Zhao, Y. Liu, T. Chen, Y. Li, B. Tang, Rationally optimized fluorescent probe for imaging mitochondrial SO₂ in HeLa cells and zebrafish, *Anal. Chem.* 90 (2018) 12442–12448.
- [46] D. Carmona-Gutierrez, A. Alavian-Ghavanini, L. Habernig, M. Bauer, A. Hammer, C. Rossmann, A. Zimmermann, C. Ruckstuhl, S. Büttner, T. Eisenberg, W. Sattler, E. Malle, F. Madeo, The cell death protease Kex1p is essential for hypochlorite-induced apoptosis in yeast, *Cell Cycle* 12 (2013) 1704–1712.
- [47] F.L. Coe, P.R. Korty, The effect of hydrazine upon renal excretion of sodium, potassium and water, *J. Pharmacol. Exp. Ther.* 161 (1968) 183–190.
- [48] T. Dambrauskas, H.H. Cornish, The distribution, metabolism, and excretion of hydrazine in rat and mouse, *Toxicol. Appl. Pharmacol.* 6 (1964) 653–663.